



# Pattern formation in fluidized beds as a tool for model validation: A two-fluid model based study



Kaiqiao Wu<sup>1</sup>, Lilian de Martín<sup>\*,1</sup>, Luca Mazzei, Marc-Olivier Coppens<sup>\*</sup>

University College London, Department of Chemical Engineering, Torrington Place, WC1E 7JE London, UK

## ARTICLE INFO

### Article history:

Received 23 April 2015

Received in revised form 23 February 2016

Accepted 8 March 2016

Available online 16 March 2016

### Keywords:

Fluidization

Structuring

CFD

Validation

Eulerian–Eulerian

Pulsation

## ABSTRACT

Computational fluid dynamics (CFD) models have been broadly used during the last twenty years to engineer and understand fluidized beds. Nevertheless, there is some controversy about the rigor of their current validation methodologies (Powder Technol. 139 (2004), 99). A robust tool to determine whether or not a model reproduces—let alone, can predict—the dynamics of a fluidized bed is still missing. This is especially relevant for the validation of the fluid-particle closures that are emerging with the help of direct numerical simulation. More than a decade ago, it was demonstrated experimentally that regular patterns emerge in pulsed fluidized beds under certain experimental conditions. These patterns are not a singular feature of the dynamics, such as average bubble size or bed expansion, but form as a result of a precise coupling between multi-scale physical phenomena. Remarkably, CFD has not been able, so far, to reproduce the experimental bubble patterns convincingly. In this work, we want to bring to the attention of the fluidization community the power of pattern formation in fluidized beds as a tool for model validation. As a proof of concept, we apply this validation test to two-fluid models. Our two-fluid simulations reproduce bubble properties reasonably well, but fail to reproduce the experimentally witnessed patterns, suggesting that the physics of the fluidized state are not correctly captured by this approach, under any of its common implementations.

© 2016 The Authors. Published by Elsevier B.V. This is an open access article under the CC BY license (<http://creativecommons.org/licenses/by/4.0/>).

## 1. Introduction

Gas–solid fluidized beds are widely used in industrial processes where good heat and mass transfer are of paramount importance. The mixing and transport properties of these reactors originate from non-linear physical phenomena occurring at multiple spatio-temporal scales, resulting in complex dynamics [1] that greatly complicate fluidized bed control and scale-up [2].

Computational fluid dynamics (CFD) has been broadly used during the last twenty years to facilitate the engineering and understanding of fluidization processes [2–6]. Two main approaches can be distinguished: two-fluid models (Eulerian–Eulerian) and discrete particle models (Eulerian–Lagrangian). In two-fluid models, both the gas and particle phases are treated mathematically as interpenetrating continua, and one solves for the local solids concentration instead of the particle trajectories [3]. Averaging the instantaneous equations in a suitable way allows one to use a coarser mesh and longer time steps, decreasing the computational effort at the cost of introducing unknowns into the governing equations. The model

must be completed by defining closure laws—topological, constitutive, and transfer laws— which can be derived from empirical information, phenomenological models and micromechanical theories. Two-fluid models are broadly used in the fluidization field since they can simulate systems up to 1 m or more in a reasonable amount of time. However, they are deemed more useful for predicting qualitative trends than absolute values mainly due to the inaccuracies of the closure laws [2].

Discrete particle models apply the discrete treatment to a dispersed phase, which is resolved by tracking particles individually following Newton's laws of motion. These models can be divided into discrete element models (DEM) and direct numerical simulations (DNS). In DEM, the mesh size of the Eulerian grid is at least one order of magnitude larger than the particle size [5]. Particles are treated as point sources and sinks of momentum, requiring the use of closures to solve the gas–particle interaction. This approach can simulate systems up to 0.1 m and help to unravel the influence of particle–particle, gas–particle, and particle–wall interactions in the formation and mixing of heterogeneous flow structures. On the contrary, the size of the Eulerian grid in DNS is at least one order of magnitude smaller than the particle size [7,8]. Gas–particle interactions are resolved by imposing a stick boundary condition at the surface of a particle. DNS is the only approach that does not require the implementation of closures, because it does not involve averaging. Although it is the most computationally expensive

\* Corresponding authors.

E-mail addresses: [ldemartin@ucl.ac.uk](mailto:ldemartin@ucl.ac.uk) (L. de Martín), [m.coppens@ucl.ac.uk](mailto:m.coppens@ucl.ac.uk) (M.-O. Coppens).

<sup>1</sup> These authors contributed equally to this work.

simulation technique, one of its appeals is that it can help to develop the closure laws for fluid–particle interactions necessary to simulate larger systems [6].

CFD validation has progressed in parallel to model development, and is subject to intense discussion [9–11]. Simple models based on empirical correlations are considered helpful when they are able to predict an experimental phenomenon under a limited range of physical conditions. More fundamental models, including the main physical mechanisms, such as the models included in commercial CFD packages, are expected to represent the process over a broad range of conditions in a more reliable way. A large variety of physical systems and models complicate a systematization of the validation procedure. In addition, the substantiation test that a model must pass to be considered valid often depends on the expectations for the model and, sometimes, even on the researchers' interests [9,11]. Grace and Taghipour [11] provided several guidelines for CFD validation in an effort to avoid the excessive claims that are common in the literature. Examples are: covering a broader range of conditions, performing proper error analysis, and seeking expert opinion to determine whether or not there is agreement between the experimental and modeled phenomenon. Some of these guidelines can be fulfilled with good experimental and numerical practices, whereas other ones remain inherently subjective. There is no consensus on how broad the experimental space must be, what phenomena the model must explain to be considered fully validated, or when simulated and experimental traits can be considered in “reasonable agreement”. Models are typically tested by comparing the experimental and theoretical bubble properties [12–16], void fraction [17,18], particle velocity [13,19–22], segregation [18], time-averaged solid/gas volume fractions [13], bed expansion [13,14], pressure fluctuations [23–25], and mass flux profiles [26]. These are different manifestations of the system dynamics that are, ultimately, what the model should be able to reproduce.

More than a decade ago, Coppens et al. [27,28] demonstrated experimentally that a pulsated gas flow could induce the formation of regular bubble patterns in gas–solid fluidized beds. In quasi-2D beds, that is, thin in one horizontal dimension, bubbles rise forming hexagonal configurations (Fig. 1), whereas, in shallow 3D beds, regular patterns form on the top surface resembling those observed in vibrated granular media [29,30]. Independently of the bed geometry, experimental bubble patterns are sub-harmonic; bubbles alternate their positions in each pulse and the pattern is repeated after two pulses. Pattern formation in fluidized beds has remained highly unexplored and is not

understood yet, although preliminary studies point at phase locking (synchronization) as a possible mechanism [27]. The theory of dynamical synchronization is too vast to be described here in detail, but the main idea is that a periodic external force can stabilize certain states of chaotic dynamics, represented by orbits in a strange attractor [31]. Hence, synchronization depends on the properties of the external force and attractor topology, such as local trajectories, and phase dynamics. Simulating synchronization in a chaotic fluidized bed requires a model that captures at least the main features of the attractor, which are intimately related to the multi-scale dynamics of the underlying physical system.

Few attempts have been made in this direction. Kawaguchi et al. [32] studied pulsed fluidization using DEM. They reported that pulsation frequencies of 4–5 Hz induced regularity in the bubble behavior for Geldart B particles. A row of two large bubbles at fixed positions was stably formed in each pulse; however, the sub-harmonic, alternating behavior that is characteristic of the experimental patterns was not observed. [33] also conducted DEM of fluidization of Geldart B particles, finding that frequencies of 5–10 Hz increased the regularity of the bubble dynamics. However, their results are far from the clear experimental patterns, something the authors attribute to the thin bed—one particle diameter—and insufficient simulation time.

It is remarkable that CFD simulations have not been able to convincingly reproduce, so far, the experimental bubble patterns. Patterns are not one feature of the dynamics, but emerge from the coupling between dynamics occurring at multiple spatio-temporal scales [34]. To reproduce the patterns, the model must capture the underlying physics of the fluidized state in a proper manner. This allows to validate CFD models based on their ability to reproduce the experimentally witnessed regular patterns. In addition, regular patterns (bubbles patterns in quasi-2D beds or surface patterns on 3D beds) are easy to identify visually, preventing the artifacts introduced by many experimental and analysis techniques, and facilitating the comparison between the modeled and experimental system. Although the synchronization phenomenon in fluidized beds is a promising tool for CFD validation, it has been largely ignored by the fluidization community, so far.

In this work, we show the power of pattern formation for CFD validation using two-fluid models as a case study. Two-fluid models are extensively used in the fluidization field [2,3,13,17,22], and their low computational effort compared to other approaches makes them a natural first choice for our purpose. More complex CFD models, such as DEM, will also be tested in the future.

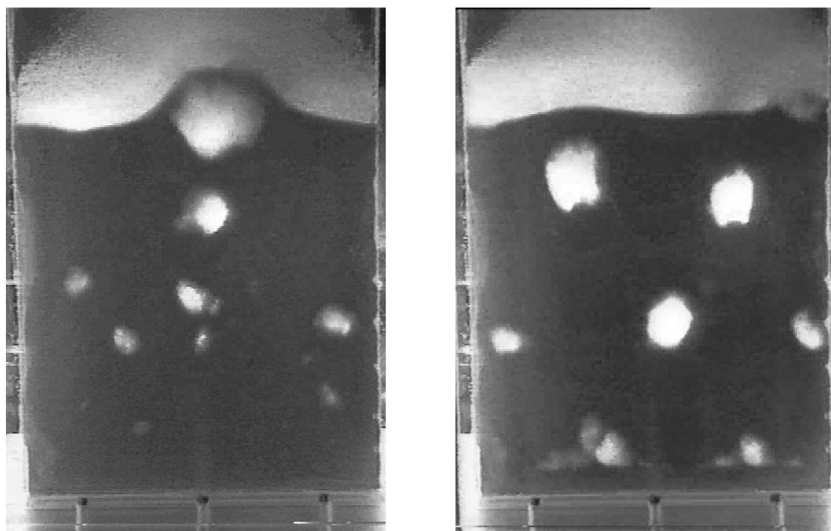


**Fig. 1.** Quasi-2D bed of sand fluidized with air at  $u_0/u_{mf} = 1.3$  (left) and  $u_0/u_{mf} = 1.3 + 0.5\sin(2\pi 4t)$  (right). The hexagonal bubble configuration generated by the oscillating flow is evident. The movies of these snapshots are included in the Supplementary Material.

## 2. Two-fluid model implementation

### 2.1. Governing equations

Two-fluid models consider both gas and solid phases as interpenetrating continua [3,2]. The governing equations describing the conservation of mass (continuity equations) and linear momentum (Navier–Stokes equations) can be found in Table 1.

The stress tensor of both phases is modeled using the Newtonian strain–stress relation  $\bar{\mathbf{T}} = -p\bar{\mathbf{I}} + \bar{\boldsymbol{\tau}}$ . The viscous contribution for the solid phase is  $\bar{\boldsymbol{\tau}}_s = \phi\mu_s[\nabla\mathbf{u}_s + (\nabla\mathbf{u}_s)^T] + \phi(\lambda_s - \frac{2}{3}\mu_s)\nabla \cdot \mathbf{u}_s\bar{\mathbf{I}}$ , where  $\mu_s$  and  $\lambda_s$  are the shear and bulk viscosity, respectively.

Particle–particle interactions are modeled according to the kinetic theory of granular flow (KTGF) [35]. This approach assumes that the motion and fluctuating kinetic energy for fluidized particles and molecules in a dense gas is analogous; therefore, the fluctuating component of particle velocity can be described defining a granular temperature,  $\Theta$ . The term  $\bar{\mathbf{T}}_s : \nabla\mathbf{u}_s$  in the balance of granular temperature (Table 1) represents conversion of mean-flow energy into fluctuating kinetic energy owing to the presence of strain. The term  $\nabla \cdot (-\kappa\nabla\Theta)$  accounts for diffusion of fluctuating kinetic energy,  $\gamma$  represents energy dissipation due to inelastic collisions, and  $3\beta\Theta$  is the net rate of transfer of fluctuation energy between the two phases [36].

The KTGF treats inter-particle collisions as instantaneous and binary, something that is satisfied in relatively dilute environments and rapid flows, i.e., the *viscous* regime. Here, particles undergo transient collisions and the momentum transfer is due to collision and translation. This regime is characterized by a solid pressure  $p'_s$  and a shear viscosity  $\mu_{s,\nu} = \mu_{s,\text{col}} + \mu_{s,\text{kin}}$  that includes the two named mechanisms for momentum transfer. On the contrary, particles in the *plastic* regime bear continuous contact instead of instantaneous collisions, leading to a frictional mechanism for momentum transfer. Classical KTGF would under-predict the solid phase pressure and viscosity in the plastic regime, so it is necessary to couple it with frictional stress models for the solid phase. The most common practical implementation is to assume that the onset to the plastic regime occurs when the solid volume fraction exceeds a frictional packing limit,  $\phi_c$ . Then,

$$\mu_s = \begin{cases} \mu_{s,\text{col}} + \mu_{s,\text{kin}} & \text{for } \phi < \phi_c \\ \mu_{s,\text{col}} + \mu_{s,\text{kin}} + \mu_{s,\text{fr}} & \text{for } \phi \geq \phi_c \end{cases} \quad (1)$$

and

$$p_s = \begin{cases} p'_s & \text{for } \phi < \phi_c \\ p'_s + p_s^{\text{fr}} & \text{for } \phi \geq \phi_c \end{cases} \quad (2)$$

Expressions for all the closures can be found in Appendix A.

### 2.2. Closures

It is out of the scope of this work to test the pattern formation capabilities of all closures available in the literature. Instead, we are narrowing down this study by focusing on some of the most common

**Table 1**  
Governing equations for two-fluid model.

Continuity equation for gas phase
$\partial_t(\rho_g\epsilon) + \nabla \cdot (\rho_g\epsilon\mathbf{u}_g) = 0$
Continuity equation for solid phase
$\partial_t(\rho_s\phi) + \nabla \cdot (\rho_s\phi\mathbf{u}_s) = 0$
Momentum conservation equation for gas phase
$\partial_t(\epsilon\rho_g\mathbf{u}_g) + \nabla \cdot (\epsilon\rho_g\mathbf{u}_g\mathbf{u}_g) = \nabla \cdot \bar{\mathbf{T}}_g + \epsilon\rho_g\mathbf{g} + \mathbf{M}_g$
Momentum conservation equation for solid phase
$\partial_t(\phi\rho_s\mathbf{u}_s) + \nabla \cdot (\phi\rho_s\mathbf{u}_s\mathbf{u}_s) = \nabla \cdot \bar{\mathbf{T}}_s + \phi\rho_s\mathbf{g} + \mathbf{M}_s$
Granular temperature equation
$\frac{3}{2}\partial_t(\phi\rho_s\Theta) + \nabla \cdot (\phi\rho_s\mathbf{u}_s\Theta) = \bar{\mathbf{T}}_s : \nabla\mathbf{u}_s - \nabla \cdot (-\kappa\nabla\Theta) - \gamma - 3\beta\Theta$

closures used in two-fluid simulations. In particular, we take the work of [22] as a representative example of a standard two-fluid approach. Since the authors conducted fluidized bed experiments also under a quasi-2D geometry, and validated many closures of two-fluid models experimentally. We use some of the closures the authors discuss there to ensure a correct combination and satisfactory performance of the two-fluid model implemented in the present work.

#### 2.2.1. Interfacial force

The interfacial momentum exchange term is assumed to consist of buoyancy and drag forces. Other components, such as Saffmann and Magnus forces are considered negligible. The drag force is modeled according to Gidaspow's correlation [37] which integrates the correlations of [38] and of Wen and Yu [39] via a switch function. The equations for the drag force closure can be found in Appendix A.5.

The total interfacial force is

$$\begin{aligned} \mathbf{M}_g &= -\beta(\mathbf{u}_g - \mathbf{u}_s) + \phi\nabla p_g & \text{for the gas phase} \\ \mathbf{M}_s &= \beta(\mathbf{u}_g - \mathbf{u}_s) - \phi\nabla p_g & \text{for the solid phase} \end{aligned} \quad (3)$$

#### 2.2.2. Frictional stress

Schaeffer's closure for the frictional viscosity [40], coupled with Syamlal's correlation for the frictional pressure [41], has been used throughout this study (Eq. (A.7)). A correct description of the plastic regime is fundamental to our simulations since some of the most stable experimental patterns occur approximately for a minimum velocity close to  $u_{\text{mf}}$  [42,28]. This implies that the bed operates periodically close to the minimum fluidization velocity, where particles are in continuous contact and frictional mechanisms dominate over kinetic and collisional ones.

### 2.3. Numerical settings

2D simulations were run in Ansys Fluent 12. The pressure-based solver was selected for low-speed incompressible flows, phase coupled SIMPLE algorithm for the relation between pressure and velocity, second-order upwind for momentum and granular temperature, first-order upwind for volume fraction, and a first order implicit scheme for temporal discretization. Gradients were calculated with a Green–Gauss node-based scheme, which adopts the arithmetic average of the nodal values on each grid cell.

A sensitivity analysis was performed to choose the optimal time step and cell size. Time steps of  $5 \times 10^{-4}$  s and  $10^{-4}$  s, and grid sizes of 2.5 mm and 5 mm did not show differences in axial bubble size profile and average bed height. Based on these results, the grid was refined with uniform square cells of 5 mm size. The time step is  $5 \times 10^{-4}$  s, with a maximum of 200 iterations per time step to ensure convergence.

### 2.4. Experimental and simulated conditions

Experimental conditions for pattern formation are taken from [42]. Experiments were conducted in a  $40 \times 1.5$  cm quasi-2D bed equipped with a porous plate distributor. Sand with a particle size distribution 230–590  $\mu\text{m}$  and average particle size of 360  $\mu\text{m}$  was fluidized with air at room conditions. The reported minimum fluidization velocity  $u_{\text{mf}}$  is 0.13 m/s. The initial bed height is approximately 40 cm. The most stable patterns were observed when operating with a 4 Hz sinusoidal flow oscillating between  $u_{\text{mf}}$  and  $1.8 u_{\text{mf}}$ .

In the simulation, the choice of the frictional packing limit  $\phi_c$  must approximate the experimental  $u_{\text{mf}}$ , since the drag force depends on the solids fraction, which, in turn, depends on  $\phi_c$ . A value of  $\phi_c = 0.6$  gives a simulated  $u_{\text{mf}}$  of 0.11 m/s, somewhat smaller than the experimental value but nearly the same as the theoretical value of 0.10 m/s obtained from Wen and Yu's correlation [39] for 360  $\mu\text{m}$  mono-disperse particles. The small difference between the experimental and

**Table 2**  
Parameters for the 2D simulations.

Parameter	Value
Particle density, $\rho_s$	2500 kg/m <sup>3</sup>
Gas density, $\rho_g$	1.225 kg/m <sup>3</sup>
Gas viscosity, $\mu_g$	$1.8 \cdot 10^{-5}$ Pa s
Particle diameter, $d_s$	360 $\mu$ m
Restitution coefficient, $e$	0.9
Angle of internal friction, $\theta$	30°
Frictional packing limit, $\phi_c$	0.6
Initial solid volume fraction, $\phi$	0.39–0.41 (random)
Bed width, $W$	40 cm
Static bed height, $H$	40 cm
Drag closure	[37]
Wall boundary condition	No-slip for both phases
Inlet boundary condition	Velocity inlet type: $u_0/u_{mf} = A + B\sin(2\pi ft)$
Outlet boundary condition	Pressure outlet type: 101,325 Pa
Time step	$5 \times 10^{-4}$ s
Cell size	5 mm

simulated  $u_{mf}$  can be attributed to the size distribution of the real solid. In addition,  $\phi_c = 0.6$  is the frictional packing limit recommended by [41] when deriving his closure and it has been used by [22] in their work, which is used as a reference.

A summary of the simulation conditions is shown in Table 2.

### 2.5. Bubble identification

In a two-fluid simulation, a bubble is defined as a region of the computational domain which comprises cells where the solid volume fraction  $\phi$  is lower than a threshold value  $\phi_b$ . Here,  $\phi_b = 0.2$  [43]. The variation of the solid volume fraction with time indicates that the steady state is reached after  $\sim 3$  s. Bubble identification is therefore carried out between 3 s and 10 s at the post-processing stage of each time step. A program was written in house to identify the bubbles in the present work. The equivalent bubble diameter is obtained from the bubble area:  $d_{eq} = \sqrt{\frac{4A_b}{\pi}}$ . A minimum equivalent bubble diameter of 1 cm, equivalent to 4 grid cells, is imposed to remove spurious bubbles.

## 3. Results and discussion

### 3.1. Validation under constant gas flow

To ensure that the simulation and closures are correctly implemented, a rudimentary validation test was performed prior to the study of pattern formation. Simulated bubble size and rising velocity are compared to the experimental values reported by [22] in a conventional quasi-2D bed under the same conditions. For this preliminary validation, the 2D computational domain is 50 cm wide  $\times$  200 cm high with a 30 cm

high initial loading of 700  $\mu$ m particles. The air velocity is constant and equal to 0.62 m/s.

In terms of bubble size growth and rising velocity, the computational and experimental results are in reasonable quantitative agreement (Fig. 2), which shows that our two-fluid implementation is able to predict basic features of a conventional fluidized bed. It is worth mentioning that bubbles in an experimental quasi-2D bed are forced to have a disk-like shape, i.e., thin in their third dimension. The simulation neglects the boundary effects from both front and back walls by adapting a quasi-2D bed to a 2D model, which, to a certain extent, might contribute to the differences in the results.

### 3.2. Oscillating gas flow

In this section, the response of the simulated bed dynamics to an oscillating flow of the form  $u_0/u_{mf} = A + B\sin(2\pi ft)$  is discussed. Variations in the flow frequency  $f$ , offset  $u_{min}/u_{mf} = A - B$ , and amplitude  $B$  are investigated. The selected values for these parameters correspond to the range where experimental bubble patterns are observed [42] (Table 3).

### 3.3. Influence of the pulsed flow frequency, $f$

Experimental bubble patterns were observed in the range of pulse frequencies 2.5–7 Hz, and were more stable in the lower part of this range [42,28]. Experimentally, bubbles still form in a sub-harmonic, regular fashion, for frequencies above 7 Hz, but they are so small that they quickly coalesce and the pattern vanishes close to the distributor. For constant average gas velocity  $A$  and offset, the bubble size decreases with the frequency due to the smaller volume of gas injected in each pulse,  $V_p \propto Au_{mf}/f$ , whereas the number of coexisting bubbles increases due to the smaller vertical bubble pitch. In addition, it was suggested that higher frequencies increase the gas volume fraction of the dense phase [42,28].

The effect of pulse frequency on the two-fluid simulation results is displayed in Fig. 3. The computational average bubble size decreases linearly from  $\sim 1.7$  cm to  $\sim 1.3$  cm, in reasonable quantitative agreement with the experimental data reported in [42] for the same oscillating flow. The better aeration of the dense phase for larger frequencies suggested in [42] is not captured by the two-fluid model.

Visual observation reveals that the most regular dynamics are obtained at around 3–4 Hz. However, at this frequency, the bed still exhibits quite chaotic behavior, with some episodes of regularity where three relatively large bubbles at fixed positions are formed at every pulse. This is similar to the observations reported by [32] in their DEM simulations, although in our case the regularity is not so stable. The alternating bubble behavior that characterizes the experimental bubble patterns is not observed at any frequency.

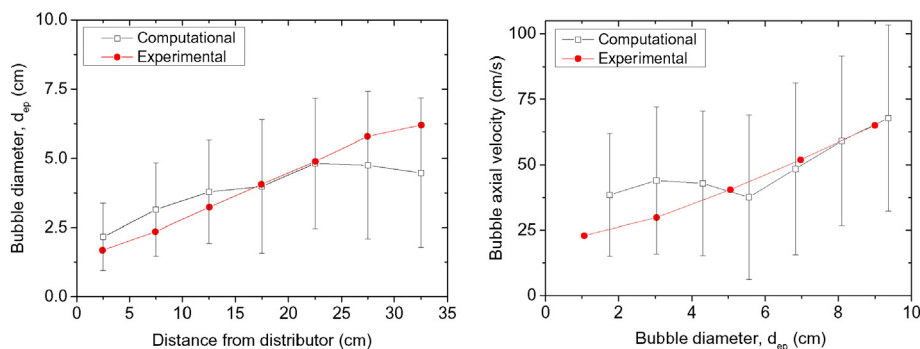


**Fig. 2.** Experimental and computational bubble size growth (left) and rising velocity (right). Experimental data are taken from [22]. The error bars represent the standard deviations. The agreement between the experimental and simulated bubble properties is satisfactory.

**Table 3**  
Inlet boundary conditions  $u_0/u_{mf} = A + B\sin(2\pi ft)$  investigated.

$f$ (Hz)	A-B	B
2–5	1	0.4
4	1	0.3, 0.4, 0.5
4	0.8, 1, 1.2	0.4

### 3.4. Influence of the pulsed flow amplitude, $B$

The clearest experimental patterns form for  $0.3 < B < 0.5$ . A smaller amplitude of the flow generates bubbles near the distributor that are too small to be stable, whereas a larger amplitude injects too much air in every pulse, generating additional bubbles that disturb the pattern. It is reported that, in a 15 cm deep bed, for a constant frequency  $f = 4$  Hz and average flow  $A = 1.4$ , the bubble size increases linearly from 1.3 cm for  $B = 0.1$ , to 1.6 cm for  $B = 0.42$  [42].

Different from [42], we test the influence of the amplitude  $B$  by keeping the flow offset  $A-B$  constant and equal to 1, instead of keeping the average  $A$  constant, as our recent insights suggest that maintaining the flow offset is more important than the average flow for pattern formation. It is observed that the computed bubble size increases with the amplitude for constant offset and frequency (Fig. 4). Considering the gas as incompressible, the equivalent bubble diameter in quasi-2D beds can be estimated from the volume of gas injected during each pulse. Assuming that the dense phase is at minimum fluidization conditions, the bubble size can be estimated from the average flow  $A$ , this is:

$$d_{eq} = \sqrt{\frac{4Wu_{mf}}{N_b\pi f}(A-1)} \quad (4)$$

where  $N_b$  is the number of bubbles generated at each pulse.

For an offset of  $A-B = 1$ , Eq. (4) converts to  $d_{eq} \propto \sqrt{\frac{B}{N_b f}}$ . Therefore,  $B$  and  $1/f$  have a similar influence on the bubble size, as these two parameters increase the volume of gas injected during each pulse.

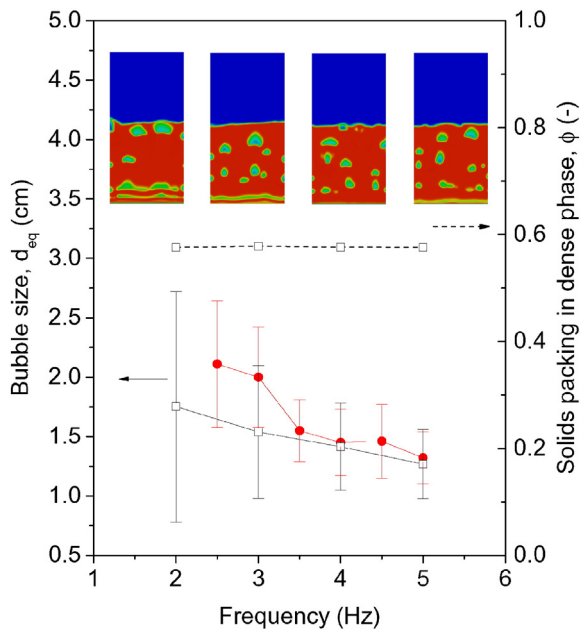


**Fig. 3.** Influence of the pulse frequency on the average bubble size (left axis) and solids packing in the dense phase (right axis). Open symbols represent computational values, whereas close symbols stand for experimental values from [42]. The error bars represent the standard deviations. Snapshots correspond to  $f = 2, 3, 4$  and  $5$  Hz, from left to right. Offset  $A-B = 1$  and amplitude  $B = 0.4$ .

It is not possible to carry out a one-to-one comparison between our simulated bubble size and Regelink's observations [42], as they keep the average flow  $A$  constant instead of the offset  $A-B$ . However, both the bubble size and trend are similar.

### 3.5. Influence of the gas velocity offset, $A-B$

Pattern formation in quasi-2D beds occurs in a very narrow range of flow offsets [42], where most stable patterns manifest themselves for a minimum flow between  $u_{mf}$  and  $1.2 u_{mf}$ . Regular patterns are also observed when working with minimum flows below  $u_{mf}$ , but they are less stable. A too small offset would completely defluidize the bed at every flow minimum; any memory about the previous dynamical state is lost and the pattern is not observed.

Both experiments and our simulations show that for a constant flow amplitude and frequency, the average bubble size grows when increasing the offset. This can be attributed to an increase of the average flow  $A$ , which in turn causes larger volume of gas to be injected in each pulse (Eq. (4)). There is good quantitative agreement between experimental and simulated bubble size (Fig. 5). The simulated bubble size shows a rapid growth when the offset is increased from 0.9 to 1 as the bed transitions from a partially to a fully fluidized state.

### 3.6. Discussion

None of the simulations conducted in this study has been able to reproduce structured bed dynamics, let alone the regular bubble patterns observed experimentally. Remarkably, our simulations would pass many of the validation tests performed in the literature, as bubble dynamics and minimum fluidization velocity are well captured for a variety of conditions. These results highlight the power of pattern formation as a tool for model validation compared to classical validation techniques.

Two-fluid models have helped to design and understand fluidized beds during the last twenty years; however, the correctness of applying a continuum approach to model granular matter, which is, inherently, intermittent, is debatable. From a practical point of view, current two-fluid models are weak at capturing the solid motion in quasi-2D beds [22]. The regular patterns emerge under circumstances where the particulate phase oscillates close to the minimum fluidized state, alternating between fluid-like and solid-like behaviors. In this regard, most of the solid–fluid alternating behavior of a patterned bed must be captured by the frictional tensor, which is key to any two-fluid model. Closures available in the literature for the frictional normal stress

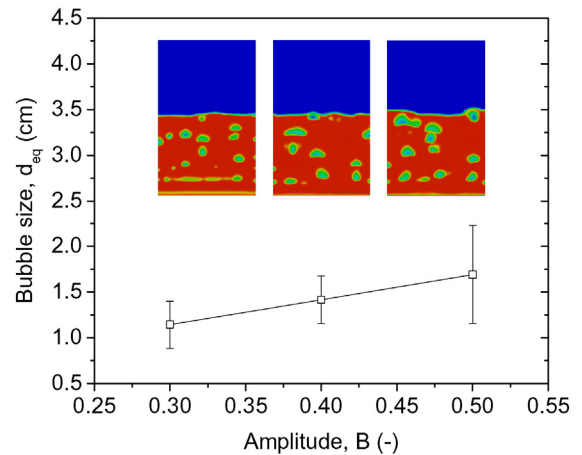


**Fig. 4.** Influence of the gas velocity offset on the average bubble size. The error bars represent the standard deviations. Snapshots correspond to  $B = 0.3, 0.4$ , and  $0.5$ , from left to right. Offset  $A-B = 1$  and frequency  $f = 4$  Hz.

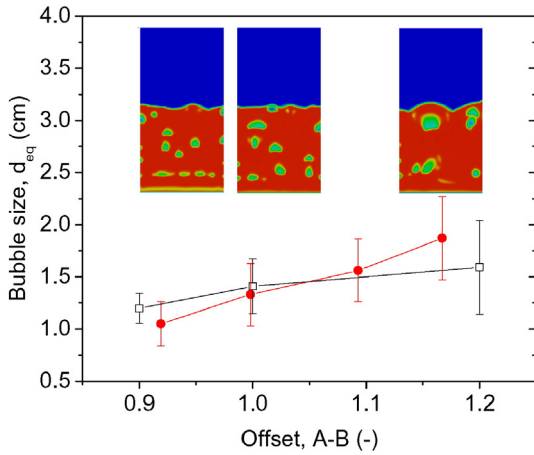


**Fig. 5.** Influence of the pulsed flow offset  $A-B$  on the fluidization dynamics. The open symbols represent the computational values, whereas the close symbols stand for the experimental values from [42]. The error bars represent the standard deviations. Snapshots correspond to  $A-B = 0.9, 1.0,$  and  $1.2$ , from left to right. Amplitude  $B = 0.4$  and frequency  $f = 4$  Hz.

might differ by orders of magnitude [4] and are, perhaps, oversimplified, especially at low fluidization velocities.

In summary, a correct prediction of local solid motion, velocity fluctuations and force chains is of significant importance to obtain these periodic patterns. A more detailed description of the solid phase, using discrete element methods, is advised to improve the prediction of the solid phase.

#### 4. Conclusions

In this paper, we have demonstrated how to apply pattern formation in fluidized beds as a tool for CFD model validation, in particular for 2D two-fluid models. It can be concluded that the representative two-fluid model implemented in this work succeeds in capturing bubble dynamics, but completely fails to reproduce the experimental regular bubble patterns. These results suggest that two-fluid approaches cannot capture the underlying physics of the fluidized state, especially at low gas velocities. This does not discredit the use of two-fluid models in general; however, they are strikingly unable to reproduce the experimentally observed bubble patterns, pointing to deficiencies in their assumptions that are relevant in practical circumstances.

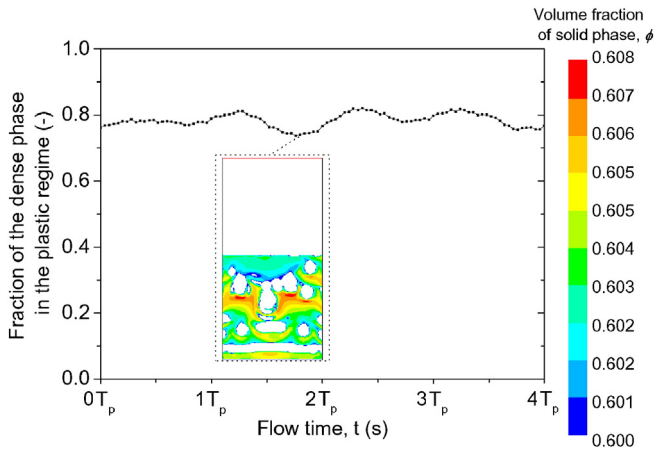


**Fig. 6.** Fraction of the dense phase in the plastic regime. The selected case corresponds to offset  $A-B = 0.4$ , amplitude  $B = 0.4$ , and frequency  $f = 4$  Hz. Data are sampled during the 10th second of simulation time, containing 4 periods of pulsation (1 s). Snapshot shows the spatial distribution of solids in the plastic regime ( $\phi > \phi_c$ ), where the frictional contribution is included.

One approach is to move towards more fundamental models, especially with the help of direct numerical simulations (DNS) and discrete element model. These are allowing to develop more accurate closures for fluid–particle interaction that can be implemented in coarser approaches. However, better descriptors of the mesoscopic physics are required as well to bridge the wide range of relevant length scales. Fundamental models should confront validation procedures tougher than those currently applied in the literature. In this context, pattern formation excels as a validation tool, or, more specifically, as a falsification test, that is a test for the null hypothesis that the model is reproducing experimentally observed fluidized bed dynamics properly.

#### Notation

$A$	average of oscillating flow, [-]
$A_b$	bubble area, [cm <sup>2</sup> ]
$B$	amplitude of oscillating flow, [-]
$C_d$	particle drag coefficient, [-]
$F$	total number of frames, [-]
$H$	bed height, [cm]
$N_b$	number of bubbles formed in each pulse, [-]
$T_p$	pulsed flow period, [s]
$V_p$	volume of gas injected in each pulse, [cm <sup>3</sup> ]
$W$	bed width, [cm]
$M$	interphase momentum exchange, [kg/(m <sup>2</sup> s <sup>2</sup> )]
$\bar{I}$	identity matrix, [-]
$\bar{T}$	stress tensor, [Pa]
$g$	gravitational acceleration, 9.8 [m/s <sup>2</sup> ]
$u$	velocity, [cm/s]
$Re$	particle Reynolds number, [-]
$d_s$	particle size, [μm]
$d_{eq}$	equivalent bubble diameter, [cm]
$e$	restitution coefficient, [-]
$f$	frequency of oscillating flow, [Hz]
$g_{0,ss}$	radial distribution function, [-]
$p$	pressure, [Pa]
$p_s^v$	viscous solid pressure, [Pa]
$p_s^{fr}$	frictional solid pressure, [Pa]
$t$	time, [s]
$u_0$	superficial gas velocity, [m/s]
$u_{mf}$	minimum fluidization velocity, [m/s]

#### Greek letters

$\beta$	drag force coefficient, [kg/(m <sup>3</sup> ·s)]
$\bar{\tau}$	shear stress tensor, [Pa]
$\varepsilon$	volume fraction of gas phase, [-]
$\gamma$	granular energy dissipation, [W/m <sup>3</sup> ]
$\kappa$	granular energy conductivity, [kg/(m·s)]
$\lambda_s$	bulk viscosity of solid, [Pa·s]
$\mu$	viscosity, [Pa·s]
$\mu_{s,col}$	collisional viscosity of solid phase, [Pa·s]
$\mu_{s,fr}$	frictional viscosity of solid phase, [Pa·s]
$\mu_{s,kin}$	kinetic viscosity of solid phase, [Pa·s]
$\mu_{s,v}$	viscosity of solid phase in viscous regime, [Pa·s]
$\phi$	volume fraction of solid phase, [-]
$\phi_b$	threshold for bubble recognition, [-]
$\phi_c$	frictional packing limit, [-]
$\phi_{max}$	maximum packing limit, [-]
$\psi$	drag force corrective function exponent, [-]
$\rho$	density, [kg/m <sup>3</sup> ]
$\Theta$	granular temperature, [m <sup>2</sup> /s <sup>2</sup> ]
$\theta$	internal friction angle, [°]

## Subscripts

<i>g</i>	gas phase
<i>s</i>	solid phase

## Acknowledgments

The authors thank V. Vikrant of the Eindhoven University of Technology (TU/e) for providing the algorithm of bubble identification used in this work. The research leading to these results has received funding from an EPSRC Frontier Engineering Award (EP/K038656/1).

## Appendix A. Closure relationships

### A.1. Bulk viscosity

The bulk viscosity expresses the resistance against compression and is zero for the gas phase. For the solid phase we follow [44]:

$$\lambda_s = \frac{4}{3} \phi \rho_s d_s g_{0,ss} (1+e) \left(\frac{\Theta}{\pi}\right)^{1/2} \quad (\text{A.1})$$

where *e* is the restitution coefficient and  $g_{0,ss}$  is the radial distribution function:

$$g_{0,ss} = \left[1 - \left(\frac{\phi}{\phi_{\max}}\right)^{1/3}\right]^{-1} \quad (\text{A.2})$$

### A.2. Solid pressure

The solid pressure  $p_s$  prevents the solid phase from overpacking. [44] derived the following expression for the solid pressure in the viscous regime from the kinetic theory of granular flow:

$$p_s^v = \phi \rho_s \Theta + 2\rho_s (1+e) \phi^2 g_{0,ss} \Theta \quad (\text{A.3})$$

[41] define the solid pressure in the plastic regime as:

$$p_s^{\text{fr}} = A(\phi - \phi_{\max})^B \quad (\text{A.4})$$

Where  $A = 10^{25}$  and  $B = 10$  as suggested in [41]. The maximum packing limit  $\phi_{\max}$  is 0.63, which corresponds to poured random packing [45].

### A.3. Shear viscosity for solid phase

The collisional and kinetic viscosities are defined according to [35]:

$$\mu_{s,\text{col}} = \frac{4}{5} \phi \rho_s d_p g_{0,ss} (1+e) \left(\frac{\Theta}{\pi}\right)^{1/2} \quad (\text{A.5})$$

$$\mu_{s,\text{kin}} = \frac{10\rho_s d_s \sqrt{\Theta\pi}}{96\phi(1+e)g_{0,ss}} \left[1 + \frac{4}{5} g_{0,ss} \phi(1+e)\right]^2 \quad (\text{A.6})$$

The frictional viscosity is modeled according to [40], which is usually coupled with Eq. (A.8):

$$\mu_{s,\text{fr}} = \frac{p_s^{\text{fr}} \sin\theta}{2\sqrt{\mathbf{S}_s : \mathbf{S}_s}} \quad (\text{A.7})$$

where  $\mathbf{S}_s = \frac{1}{2} [\nabla \mathbf{u}_s + (\nabla \mathbf{u}_s)^T] - \frac{1}{3} (\nabla \cdot \mathbf{u}_s) \mathbf{I}$ .

### A.4. Diffusion of fluctuating kinetic energy

The [35] model is used for the diffusion coefficient of fluctuating kinetic energy:

$$\kappa = \frac{150\rho_s d_s \sqrt{\Theta\pi}}{384(1+e)g_{0,ss}} \left[1 + \frac{6}{5} \phi g_{0,ss} (1+e)\right]^2 + 2\rho_s \phi^2 d_s (1+e) g_{0,ss} \left(\frac{\Theta}{\pi}\right)^{1/2} \quad (\text{A.8})$$

The collisional dissipation of energy is modeled according to [44]:

$$\gamma = \frac{12(1-e^2)g_{0,ss}}{d_s \sqrt{\pi}} \rho_s \phi^2 \Theta^{3/2} \quad (\text{A.9})$$

### A.5. Drag force

The drag coefficient is calculated using the closure developed by [37]. In the very dilute regions of the bed ( $\varepsilon > 0.8$ ):

$$\beta = \frac{3}{4} C_d \frac{\rho_g \|\mathbf{u}_g - \mathbf{u}_s\| \varepsilon \phi}{d_s} \varepsilon^\psi \quad (\text{A.10})$$

where

$$\psi = -2.65 \quad (\text{A.11})$$

$$C_d = \frac{24}{\varepsilon \text{Re}} \left[1 + 0.15(\varepsilon \text{Re})^{0.687}\right] \quad (\text{A.12})$$

The relative Reynolds number is defined as:

$$\text{Re} \equiv \frac{\rho_g}{\mu_g} \|\mathbf{u}_g - \mathbf{u}_s\| d_s \quad (\text{A.13})$$

When  $\varepsilon \leq 0.8$ , the drag coefficient takes the form as:

$$\beta = 150 \frac{\phi(1-\varepsilon)\mu_g}{\varepsilon d_s^2} + 1.75 \frac{\rho_g \phi \|\mathbf{u}_g - \mathbf{u}_s\|}{d_s} \quad (\text{A.14})$$

## Appendix B. Supplementary data

Supplementary data to this article can be found online at <http://dx.doi.org/10.1016/j.powtec.2016.03.011>.

## References

- [1] C.S. Daw, C.E.A. Finney, M. Vasudevan, N.A. van Goor, K. Nguyen, D.D. Bruns, E.J. Kostelich, C. Grebogi, E. Ott, J.A. Yorke, Self-organization and chaos in a fluidized bed, *Phys. Rev. Lett.* 75 (1995) 2308–2311.
- [2] S. Pannala, M. Syamlal, T.J. O'Brien, *Computational Gas–solids Flows and Reacting Systems: Theory, Methods and Practice*, IGI Global, 2011.
- [3] H. Enwald, E. Peirano, A.-E. Almstedt, Eulerian two-phase flow theory applied to fluidization, *Int. J. Multiphase Flow* 22 (1996) 21–66.
- [4] B.G.M. van Wachem, J.C. Schouten, C.M. van den Bleek, R. Krishna, J.L. Sinclair, Comparative analysis of CFD models of dense gas–solid systems, *AIChE J.* 47 (2001) 1035–1051.
- [5] N.G. Deen, M. Van Sint Annaland, M.A. Van der Hoef, J.A.M. Kuipers, Review of discrete particle modeling of fluidized beds, *Chem. Eng. Sci.* 62 (2007) 28–44.
- [6] M.A. van der Hoef, M. van Sint Annaland, N.G. Deen, J.A.M. Kuipers, Numerical simulation of dense gas–solid fluidized beds: a multiscale modeling strategy, *Annu. Rev. Fluid Mech.* 40 (2008) 47–70.
- [7] S. Tenneti, S. Subramaniam, Particle-resolved direct numerical simulation for gas–solid flow model development, *Annu. Rev. Fluid Mech.* 46 (2014) 199–230.
- [8] N.G. Deen, J.A.M. Kuipers, Direct numerical simulation (DNS) of mass, momentum and heat transfer in dense fluid–particle systems, *Curr. Opin. Chem. Eng.* 5 (2014) 84–89.
- [9] G.B. Kleindorfer, L. O'Neill, L. Gansehan, Validation in simulation: various positions in the philosophy of science, *Manag. Sci.* 44 (1998) 1087–1099.
- [10] W.L. Oberkampf, T.G. Trucano, Verification and validation in computational fluid dynamics, *Prog. Aerosp. Sci.* 38 (2002) 209–272.

- [11] J.R. Grace, F. Taghipour, Verification and validation of CFD models and dynamic similarity for fluidized beds, *Powder Technol.* 139 (2004) 99–110.
- [12] I. Hulme, E. Clavelle, L. van der Lee, A. Kantzas, CFD modeling and validation of bubble properties for a bubbling fluidized bed, *Ind. Eng. Chem. Res.* 44 (2005) 4254–4266.
- [13] H. Lindborg, M. Lysberg, H.A. Jakobsen, Practical validation of the two-fluid model applied to dense gas–solid flows in fluidized beds, *Chem. Eng. Sci.* 62 (2007) 5854–5869.
- [14] M.J.V. Goldschmidt, R. Beetstra, J.A.M. Kuipers, Hydrodynamic modelling of dense gas–fluidized beds: comparison and validation of 3D discrete particle and continuum models, *Powder Technol.* 142 (2004) 23–47.
- [15] A. Busciglio, G. Vella, G. Micale, L. Rizzuti, Analysis of the bubbling behaviour of 2D gas solid fluidized beds: Part II. Comparison between experiments and numerical simulations via digital image analysis technique, *Chem. Eng. J.* 148 (2009) 145–163.
- [16] F. Vejehati, N. Mahinpey, N. Ellis, M.B. Nikoo, CFD simulation of gas–solid bubbling fluidized bed: a new method for adjusting drag law, *Can. J. Chem. Eng.* 87 (2009) 19–30.
- [17] A. Boemer, H. Qi, U. Renz, Eulerian simulation of bubble formation at a jet in a two-dimensional fluidized bed, *Int. J. Multiphase Flow* 23 (1997) 927.
- [18] V. Mathiesen, T. Solberg, B. Hjertager, An experimental and computational study of multiphase flow behavior in a circulating fluidized bed, *Int. J. Multiphase Flow* 26 (2000) 387.
- [19] J. Jung, D. Gidaspow, Bubble computation, granular temperatures, and Reynolds stresses, *Chem. Eng. Commun.* 193 (2006) 946–975.
- [20] S. Dan, W. Jianzhi, L. Huilin, Z. Yunhua, C. Juhui, D. Gidaspow, C. Ming, Numerical simulation of gas–particle flow with a second-order moment method in bubbling fluidized beds, *Powder Technol.* 199 (2010) 213–225.
- [21] S.H. Hosseini, G. Ahmadi, R. Rahimi, M. Zivdar, M.N. Esfahany, CFD studies of solids hold-up distribution and circulation patterns in gas–solid fluidized beds, *Powder Technol.* 200 (2010) 202–215.
- [22] F. Hernández-Jiménez, S. Sánchez-Delgado, A. Gómez-García, A. Acosta-Iborra, Comparison between two-fluid model simulations and particle image analysis & velocimetry (PIV) results for a two-dimensional gas–solid fluidized bed, *Chem. Eng. Sci.* 66 (2011) 3753–3772.
- [23] R.W. Lyczkowski, I.K. Gamwo, F. Dobran, Y. Ai, B. Chao, M. Chen, D. Gidaspow, Validation of computed solids hydrodynamics and pressure oscillations in a bubbling atmospheric fluidized bed, *Powder Technol.* 76 (1993) 65–77.
- [24] B.G.M. van Wachem, J.C. Schouten, R. Krishna, C.M. van den Bleek, Validation of the Eulerian simulated dynamic behaviour of gas–solid fluidized beds, *Chem. Eng. Sci.* 54 (1999) 2141–2149.
- [25] B.G.M. van Wachem, J. van der Schaaf, J.C. Schouten, R. Krishna, C.M. van den Bleek, Experimental validation of Lagrangian–Eulerian simulations of fluidized beds, *Powder Technol.* 116 (2001) 155–165.
- [26] R. Panday, L.J. Shadle, M. Shahnam, R. Cocco, A. Issangya, J.S. Spenik, J.C. Ludlow, B. Gopalan, F. Shaffer, M. Syamlal, C. Guenther, S.R. Karri, T. Knowlton, Challenge problem: 1. Model validation of circulating fluidized beds, *Powder Technol.* 258 (2014) 370–391.
- [27] Y. Cheng, S. Kaart, C.M. van den Bleek, M.-O. Coppens, Control of chaotic dynamics in a 2D fluidized bed by periodic gas injection, in: L. Glicksman (Ed.) *Proc. of AIChE Annual Meeting*, 31 1999, pp. 312–319.
- [28] M.-O. Coppens, M.A. Regelink, C.M. van den Bleek, Pulsation induced transition from chaos to periodically ordered patterns in fluidized beds, *Proc. of 4th World Conf. on Part. Technol. (WCPT-2002)*, Paper 355 2002, pp. 1–8.
- [29] J.R. de Bruyn, C. Bizon, M.D. Shattuck, D. Goldman, J.B. Swift, H.L. Swinney, Continuum-type stability balloon in oscillated granular layers, *Phys. Rev. Lett.* 81 (1998) 1421–1424.
- [30] C. Bizon, M.D. Shattuck, J.B. Swift, W.D. McCormick, H.L. Swinney, Patterns in 3D vertically oscillated granular layers: simulation and experiment, *Phys. Rev. Lett.* 80 (1998) 57–60.
- [31] A. Pikovsky, M. Rosenblum, J. Kurths, *Synsynchronization. A universal concept in nonlinear sciences*, Cambridge Univ Press, 2001.
- [32] T. Kawaguchi, A. Miyoshi, T. Tanaka, Y. Tsuji, Discrete Particle Analysis of 2D Pulsating Fluidized Bed, *Proc. of 4th Int. Conf. on Multiphase Flow*, 838, 2001.
- [33] X.S. Wang, M.J. Rhodes, Pulsed fluidization—a DEM study of a fascinating phenomenon, *Powder Technol.* 159 (2005) 142–149.
- [34] M. Cross, H. Greenside, *Pattern Formation and Dynamics in Nonequilibrium Systems*, Cambridge Univ Press, 2009.
- [35] D. Gidaspow, *Multiphase Flow and Fluidization: Continuum and Kinetic Theory Descriptions*, Academic Press, 1994.
- [36] J. Ding, D. Gidaspow, A bubbling fluidization model using kinetic theory of granular flow, *AIChE J.* 36 (1990) 523–538.
- [37] D. Gidaspow, R. Bezburuah, J. Ding, *Hydrodynamics of Circulating Fluidized Beds: Kinetic Theory Approach*, *Proc. of the 7th Engineering Foundation Conference on Fluidization* 1990, pp. 75–82.
- [38] S. Ergun, Fluid flow through packed columns, *Chem. Eng. Prog.* 48 (1952).
- [39] C. Wen, Y. Yu, *Mechanics of Fluidization*, *Chem. Eng. Prog. Symp. Ser.* 62 (1966) 100.
- [40] D.G. Schaeffer, Instability in the evolution equations describing incompressible granular flow, *J. Differ. Equ.* 66 (1987) 19–50.
- [41] M. Syamlal, W. Rogers, T.J. O'Brien, *Mix Documentation: Theory Guide*, National Energy Technology Laboratory, Department of Energy, Technical Note DOE/METC-95/1013 and NTIS/DE95000031, 1993.
- [42] M. Regelink, *Formation of Regular Bubble Patterns in Periodically Pulsed Gas–Solid Fluidized Beds* (Master's thesis, TUDelft) 2000.
- [43] A. Passalacqua, L. Marmo, A critical comparison of frictional stress models applied to the simulation of bubbling fluidized beds, *Chem. Eng. Sci.* 64 (2009) 2795–2806.
- [44] C.K.K. Lun, S.B. Savage, D.J. Jeffrey, N. Chepurini, Kinetic theories for granular flow: inelastic particles in Couette flow and slightly inelastic particles in a general flow field, *J. Fluid Mech.* 140 (1984) 223–256.
- [45] F.A.L. Dullien, *Porous Media: Fluid Transport and Pore Structure*, Academic Press Inc, 1992.